

Oxygen isotopic composition and U-Pb discordance in zircon

AMANDA L. BOOTH,^{1,*} YEHOShUA KOLODNY,² C. PAGE CHAMBERLAIN,¹ MICHAEL MCWILLIAMS,¹ AXEL K. SCHMITT,³ and JOSEPH WOODEN⁴

¹Department of Geological and Environmental Sciences, Stanford University, Stanford, CA 94305-2115, USA

²Institute of Earth Sciences, Hebrew University, Jerusalem, Israel 91904

³Department of Earth and Space Sciences, University of California, Los Angeles, CA 90095-1567, USA

⁴U.S. Geological Survey, 345 Middlefield Road, Menlo Park, CA 94025, USA

(Received January 14, 2005; accepted in revised form May 16, 2005)

Abstract—We have investigated U-Pb discordance and oxygen isotopic composition of zircon using high-spatial resolution $\delta^{18}\text{O}$ measurement by ion microprobe. $\delta^{18}\text{O}$ in both concordant and discordant zircon grains provides an indication of the relationship between fluid interaction and discordance. Our results suggest that three characteristics of zircon are interrelated: (1) U-Pb systematics and concomitant age discordance, (2) $\delta^{18}\text{O}$ and the water-rock interactions implied therein, and (3) zircon texture, as revealed by cathodoluminescence and BSE imaging. A key observation is that U-Pb-disturbed zircons are often also variably depleted in ^{18}O , but the relationship between discordance and $\delta^{18}\text{O}$ is not systematic. $\delta^{18}\text{O}$ values of discordant zircons are generally lighter but irregular in their distribution. Textural differences between zircon grains can be correlated with both U-Pb discordance and $\delta^{18}\text{O}$. Discordant grains exhibit either a recrystallized, fractured, or strongly zoned CL texture, and are characteristic of ^{18}O depletion. We interpret this to be a result of metamictization, leading to destruction of the zircon lattice and an increased susceptibility to lead loss. Conversely, grains that are concordant have less-expressed zoning and a smoother CL texture and are enriched in ^{18}O . From this it is apparent that various stages of water-rock interaction, as evidenced by systematic variations in $\delta^{18}\text{O}$, leave their imprint on both the texture and U-Pb systematics of zircon. Copyright © 2005 Elsevier Ltd

1. INTRODUCTION

Discordance is a common phenomenon in zircon U-Pb geochronology, and an understanding of the mechanisms for lead loss and causes for discordance in zircon continues to be important. Wetherill (1956) first proposed the concordia diagram to interpret discordant U-Pb ages, and thousands of zircon analyses performed since then support the general conclusion that although many ages are concordant (i.e., the $^{206}\text{Pb}/^{238}\text{U}$ age and the $^{207}\text{Pb}/^{235}\text{U}$ age agree within their margins of error), most are not. Discordant analyses typically plot below the concordia in linear arrays that intercept the concordia at two points. The geologic meaning of the upper intercept is almost universally considered to represent crystallization age, but the meaning of the lower intercept is much more controversial. Commonly invoked interpretations are episodic Pb loss and continuous Pb diffusion (for a review see Davis et al., 2003; Mezger and Krogstad, 1997).

It is likely that Pb removal in zircon is accomplished by an aqueous phase (Goldich and Mudrey, 1975) whose interaction may be recorded in the isotopic composition of oxygen (Taylor, 1977; for summary see Taylor and Sheppard, 1986). Here, we use $\delta^{18}\text{O}$ of zircon to identify water-rock interaction as a possible agent of Pb removal.

Modern techniques for U-Th-Pb zircon analysis include secondary ion mass spectrometry (SIMS), laser ablation inductively coupled plasma mass spectrometry (LA-ICPMS), and thermal ionization mass spectrometry (TIMS). Each technique has unique advantages. SIMS offers excellent spatial resolution

but has reduced precision and strongly depends on well characterized reference materials to correct for instrumental bias. LA-ICPMS is faster than SIMS but less sensitive, resulting in reduced spatial resolution and precision. Traditional TIMS offers excellent precision owing to the large amounts of material ionized. However, the bulk dissolution and chemical separation required for conventional TIMS compromises spatial resolution and speed. Our investigation of the relationship between U-Pb discordance and oxygen isotopic composition required documentation of intergrain and intragrain variations in $\delta^{18}\text{O}_{\text{zircon}}$; therefore we utilized the high-spatial resolution of SIMS in combination with electron beam imaging techniques including cathodoluminescence (CL) and backscattered electrons (BSE).

1.1. Oxygen Isotopes in Zircon

The potential for $\delta^{18}\text{O}$ analysis of zircon has been recognized for some time, but relatively few analyses were made until the past decade. Numerous studies have been performed more recently, primarily by workers at the University of Wisconsin. Analysis by conventional methods was problematic because the ZrF_4 produced by fluorination boils at 900° and freezes at 600° , forming a solid deposit that damages the fluorination line valve upon contact. This problem was solved in 1974 when Y. Kolodny analyzed a set of zircons obtained from L. Silver by introducing a cold U-trap between each reaction vessel and the valve above that vessel. The authors do not consider it important to reference this claim; however, details for these first analyses are presented below in the Methods section (2.2).

Among others, four well studied zircon concentrates from

* Author to whom correspondence should be addressed (mbooth@pangea.stanford.edu).

Table 1. Zircon oxygen isotopic analyses of Y. Kolodny in 1974. Samples KZ7, 8, 9, 10, 18 (the Marble Mountain suite) are plotted on Fig. 1. Details of the Pacoima zircon analyses are tabulated in EA1.

Sample #	Description	U (ppm)	$\delta^{18}\text{O}$ (#1)	$\delta^{18}\text{O}$ (#2)	$\delta^{18}\text{O}$ (avg)
KZ1	Ceylon zircon, 50 mesh; metamorphic, extremely radioactive; only slightly disturbed U-Pb system		9.2	10.3	9.8
KZ2	Kimberly zircon, slightly radioactive		4.2	3.9	4.1
KZ3	Tahawus (Adirondack Mountains, New York); granulite facies gabbro		7.5	7.6	7.6
KZ4	Baja California tonalite (BC-I-12); unmetamorphosed, 112 Ma		5.4	5.9	5.6
KZ5	Baja California granite	695	4.4	4.2	4.3
KZ6	Sheeprock granite (Utah); ~19 Ma; nonmetamorphosed, extremely high radioactivity		4.7	5.0	4.9
KZ7	Marble Mtn. Precambrian metamorphic granite	1100	5.5	5.8	5.6
KZ8	Marble Mtn. Precambrian metamorphic granite	723	6.6	7.1	6.9
KZ9 ^a	Marble Mtn. Precambrian metamorphic granite	723	7.1	6.6	6.9
KZ10 ^a	Marble Mtn. Precambrian metamorphic granite	1700	5.1	5.1	5.1
KZ11	Peninsular ranges batholith; 116 Ma; unmetamorphosed	1111	4.5	4.2	4.3
KZ12	Retrograded granulite	305	6.9	6.7	6.8
KZ13 ^b	Soledad Block metamorphic pegmatite		3.4		3.4
KZ14	Charnockite with igneous zircons (Essex county, NY); granulite facies	1400	7.7	8.2	7.9
KZ15	Quartzite in a pyroxenite-granulite terrane (Hamilton county, NY)	392	6.0	5.7	5.9
KZ16 ^b	Aibo granite (Sonoma, Mexico) micrographic granite; turbid feldspars	550	5.6		5.6
KZ17	Aibo granite (Sonoma, Mexico) micrographic granite; turbid feldspars	363	4.8	5.3	5.1
KZ18	Marble Mtn. Precambrian metamorphic granite	982	6.4	6.8	6.6
STD ^c	Pacoima zircon (crystal separate); highly differentiated pegmatite from anorthositic complex	210	4.9	4.9	4.9

^a Unmetamorphosed by major assemblage but highly disturbed U-Pb system. 1430 ± 10 Ma; isotopically disturbed at 160 ± 10 Ma

^b Only one oxygen measurement

^c 11 repeats (see the electronic annex (EA/1)).

Marble Mountains, San Bernardino County, California (Silver, 1963; Silver and Deutsch, 1963) were analyzed (Table 1). Previous work has shown discordance of U-Pb ages to be strongly correlated with both magnetic susceptibility of the zircons and U content (Silver, 1963). In four zircon concentrates from Marble Mountains, $\delta^{18}\text{O}$ is inversely related to U content (Fig. 1), suggesting that the more discordant zircons are also more depleted in ^{18}O .

Bibikova et al. (1982) analyzed the isotopic composition of oxygen in 13 zircons from a range of igneous and metamorphic

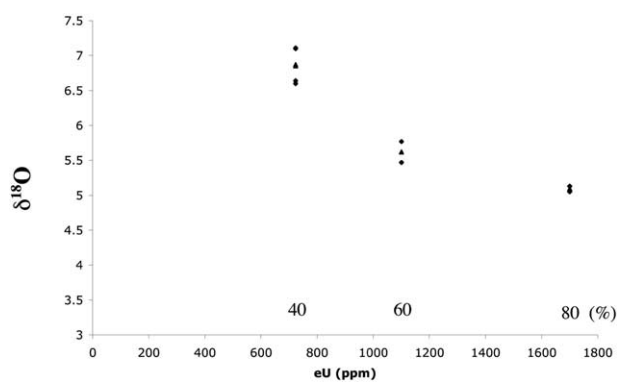


Fig. 1. Relationship between $\delta^{18}\text{O}$ and uranium content, expressed as “equivalent uranium” (eU), in several zircon fractions, from Marble Mountains, San Bernardino County, California. Equivalent uranium is defined as the total radioactivity (i.e., including Th) expressed as the equivalent uranium in ppm. Uranium contributes ~85% of the total radioactivity in these zircons (Silver, 1963). Silver (1963) presents also the relationship between eU, $^{208}\text{Pb}/^{238}\text{U}$, and degree of discordance for these same samples. The marked percentage of discordance on the inner side of the abscissa is an estimate measured from Silver’s published plots.

rocks. They noted that the least discordant zircons (which had apparently received the lowest radiation dose) had $\delta^{18}\text{O}$ values in the range 5.6‰ to 7.1‰, whereas the more discordant zircons, which were also more metamict, had lighter $\delta^{18}\text{O}$ values, reaching as low as 0.8‰.

Following the development of techniques for laser fluorination of very small samples, as well as in situ analysis by ion microprobe, $\delta^{18}\text{O}$ has now been measured in many zircons, primarily by Valley et al. (1994, 1998, 2003); Eiler et al. (1997); Peck et al. (2001, 2003); and Valley (2003). Among numerous observations, Valley (2003) noted that for zircons from the Adirondack Highlands, $\delta^{18}\text{O}$ is heavier in zircons with lower magnetic susceptibility, lower U content, and more concordant ages. Valley (2003) also summarized conclusions from Valley et al. (1994), which correlated microcracks to resetting of oxygen, age discordance, and Pb loss.

1.2. Zircon Morphology

The relationship between U-Pb systematics and zircon morphology has been repeatedly examined. Following the pioneering study of Silver and Deutsch (1963), the general approach to this question (e.g., Connelly, 2000) has been to assume that the oscillatory zoning usually revealed by cathodoluminescence represents a primary crystallization feature. Absence of zoning implied that secondary processes have affected the crystal. The absence of zoning might then be correlated with the loss of selected elements from the lattice. Connelly (2000) observed that whereas crystals with sharp oscillatory zoning (Sample 2, Fig. 1 of Connelly, 2000) are concordant, the disappearance of zoning is accompanied by age discordance. Pidgeon (1992) observed the reverse relationship: Examining zircons from the late Achaean granite of Jack Hills, Western Australia, he showed that where zoning has been obliterated, the data plot on

the concordia line, whereas the well zoned zircons are discordant to varying degrees. Pidgeon (1992) suggested that this results from early recrystallization shortly after the completion of initial magmatic crystallization, accompanied by loss of U, Th, and Pb and the removal of oscillatory zoning. The recrystallized (and unzoned) zircons are then more stable than the zoned crystals with respect to later Pb loss, and essentially have a reset zircon U-Pb age. During later disturbance events, the zoned crystals preferentially lose lead and become discordant. Pidgeon et al. (1998) further investigated the phenomenon of zoning in zircons by etching with HF vapor to reveal zoning, yielding results similar to those observed by BSE imagery. Pidgeon et al. (1998) show that dark zones (which are more susceptible to HF etching) are strongly enriched in several trace elements (U, Yb, Y, Pb, P, Ca, Ce). They explain this as primary oscillatory zoning, subsequently modified by recrystallization. This recrystallization involves migration of trace elements, from outer primary zones to inner primary zones, forming new high-concentration trace element bands. In addition, Pidgeon et al. (1998) advocate a reaction between zircon and external hydrous fluids formed during cooling of the granite.

2. SAMPLES AND METHODS

The goal of our study was to determine the relationship between discordance and $\delta^{18}\text{O}$ in zircon. We selected three samples that had previously been analyzed for U and Pb using the SHRIMP-RG at Stanford University. Zircon populations from these samples met three criteria: (1) They were widely distributed on the discordia, (2) sufficient zircon for oxygen isotope analysis was available after the SHRIMP sputter pit was removed by regrinding and polishing, and (3) visual documentation of individual grains by transmitted light, reflected light, and cathodoluminescence was available.

2.1. Sample Descriptions

Sample IG2D-01 is from the Namche Barwa region of the eastern Himalayan syntaxis, characterized by rapid uplift, intense erosion by the Yarlung Tsangpo, and a <10 Ma melting event (Booth et al., 2004). Here, basement rock consists of amphibolite to granulite-grade metapelites, intruded by small-scale (<1 m) granitic dikes and sills. IG-2D represents one such dike.

Samples SG04744 and SG04746 are both from the Lake Victoria Greenstone Belt in Tanzania, where Archean rocks are now preserved in a well developed lateritic environment (Borg and Shackleton, 1997). Zircons were separated from rocks that underwent at least three major weathering episodes. SG04744 is from a foliated quartz/two-feldspar granitoid clast within a Late Archean conglomerate outcrop. Clasts in this conglomerate are well rounded, mostly cobble and boulder-sized, and poorly bedded and sorted. Clast SG04744 shows the strongest penetrative foliation, and its precursor granite apparently experienced deformation, uplift, and erosion before being entrained in the North Mara Series conglomerate. A second sample (SG04746) is from bed-rock granitic gneiss, sampled from a locality in which the observed gneisses are boudined and folded. The interpretation of contact relations between gneiss and amphibolite remains ambiguous; SG04746 represents either basement gneisses or felsic intrusions that have incorporated bands of amphibolite xenoliths.

2.2. Methods

SHRIMP-RG measurement spots on zircon grains were documented on photographic maps. The original mounts were then repolished to remove any trace of the analysis pits and subsequently Au-coated. Oxygen isotopic measurements were made using the CAMECA ims1270 ion microprobe at UCLA. A $10 \times 20 \mu\text{m}$ oval Cs^+ primary beam with a primary intensity of $\sim 5 \text{ nA}$ was focused on the same area

of the grains previously analyzed for U-Th-Pb isotopes. Secondary ion intensities for $^{16}\text{O}^-$ and $^{18}\text{O}^-$ were simultaneously collected in Faraday cups (FC) using the CAMECA ims1270 multicollector set-up for a mass resolving power of ~ 2000 , sufficient for resolving hydride interferences from the $^{18}\text{O}^-$ peak (Fayek et al., 2002). Under these conditions, $\sim 5 \times 10^6$ counts per second were detected for the minor isotope. Following ~ 3 min presputtering to remove potentially contaminated surface material, counts were accumulated for 100 s. Raw intensities were corrected for FC backgrounds, which were measured intermittently throughout the analysis period. Background corrections were typically $<0.4\%$, and raw $\delta^{18}\text{O}$ values were within $<2\%$ of the laser fluorination values for Pacoima and AS57 zircons (see the electronic annex (EA1)). Instrumental mass fractionation was determined by replicate analysis of Pacoima zircon. Three blocks of standard measurements were acquired: at the beginning of the first ~ 12 h session and at the beginning and towards the end of the second ~ 14 h session. For individual sessions, the standard deviation for Pacoima oxygen isotope ratios was 0.53% ($n = 12$) and 0.63% ($n = 13$), respectively. No shift in instrumental mass fractionation was detected between the two blocks of measurements in the second session, but the average isotopic ratio was $\sim 1.4\%$ heavier compared to the first session. Consequently, instrumental mass fractionation was determined by averaging all Pacoima measurements for each individual session.

Three sets of bulk oxygen isotope data are available for Pacoima zircon (two reported in this study, Table 1 and EA1; Valley, 2003). The first is zircon from the Pacoima pegmatite, a bulk sample of which was measured in 1974. The samples were analyzed by reaction with fluorine gas (F_2) overnight at 600°C . The routine standard that was analyzed was Caltech Rose Quartz, with an accepted value of $\delta^{18}\text{O} = 8.43\%$ (vs. SMOW). A U-shaped steel trap was added between the Ni vessel and the valve above it. During collection the trap was kept at LN_2 temperature. Pacoima zircon was analyzed 11 times, each sample size measuring 25–35 mg, and yielding an average $\delta^{18}\text{O} = 5.25\%$, with $\sigma = 0.8\%$ vs. SMOW (EA1). Recently, seven replicate analyses of Pacoima zircon (from a different batch) performed by laser fluorination in the Stanford stable isotope biogeochemistry laboratory yielded an average of $5.74 \pm 0.11\%$ (1σ ; EA1). Valley (2003), p. 361, reports a value of 5.69% for the Pacoima pegmatite zircon (yet another batch). The most reliable “true value,” i.e., the value which we accept and correct to, is probably the one obtained on the same concentrate of zircons as the one from which the mounts were prepared, so we referenced our analyses to that value (5.7%).

The second standard we used was AS57 (1099 Ma), routinely analyzed as a standard for U/Pb analysis and incorporated in two of the three mounts that we studied. AS57 is very homogeneous in $\delta^{18}\text{O}$; later analysis (on the same separate different grains) by laser fluorination yielded a value of $\delta^{18}\text{O} = 5.2 \pm 0.3\%$ (1σ ; EA1). The corrected average $\delta^{18}\text{O}$ for AS57 is accurate within a precision estimated from replicate measurements of Pacoima zircon (Fig. 2). For isotopic measurements by SIMS, potential bias arises in the form of mismatch between reference and sample materials that in the case of zircon include: (1) compositional variation in minor components such as HfO_2 , (2) amorphization due to metamictization and, intimately related to this, (3) the presence of H_2O . For high-energy oxygen ions, Peck et al. (2001) report variations in SIMS instrumental mass fractionation of $\sim 1\%$ per 1 wt.% HfO_2 . For similar analytical conditions, differences in isotopic fractionation between crystalline materials and compositionally equivalent anhydrous and hydrous (~ 7 wt.% H_2O) glasses are in the order of $+1\%$ to -4% (Eiler et al., 1997). Our study reports results from measurements of low-energy oxygen ions, for which the magnitude of matrix effects is typically three to five times smaller than for high-energy secondary ions (Riciputi et al., 1998). Electron microprobe analyses are presented in the electronic annex (EA2) and indicate minor variability in HfO_2 for Pacoima (~ 0.9 wt.%), AS57 (1.2 wt.%), and sample zircons (1.0–2.5 wt.%; EA2). Analytical totals average 100 wt.%, with the exception of type B zircons from sample IG2D-01, where some analytical totals are as low as ~ 96 wt.% (EA2). Based on the minor compositional variations determined by electron probe analysis, we tentatively conclude that the magnitude for bias resulting from the use of Pacoima reference zircon is within the order of stated analytical uncertainties and consequently no additional corrections were performed.

Whole-rock, quartz, zircon, garnet, and feldspar oxygen isotope

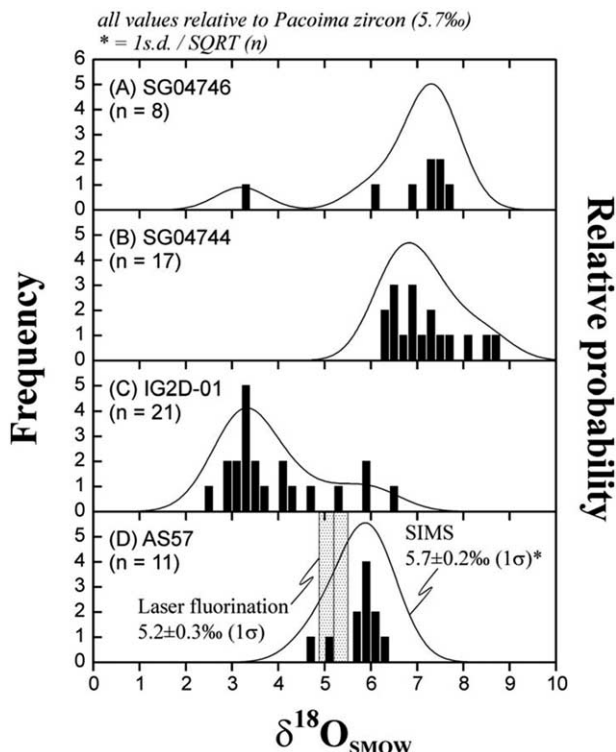


Fig. 2. Histograms and relative probability curves for SIMS $\delta^{18}\text{O}$ values of zircon from samples SG04744 and SG04746 (Tanzania; A, B), IG2D-01 (Tibet; C), and AS57 (standard zircon; D). All SIMS analyses corrected for instrumental mass fractionation using Pacoima zircon (see text). Note unimodal distribution of AS57 analyses that overlaps with the laser-fluorination values within error. The probability curves for $\delta^{18}\text{O}$ values of Tibetan and Tanzanian samples, by contrast, are skewed or multimodal.

analyses were performed at Stanford University on 0.5 to 0.8 mg separates, by heating with a CO_2 -infrared laser in the presence of BrF_5 (Sharp, 1990). Oxygen gas was directly analyzed using a Finnigan MAT 252 mass spectrometer and isotopic values corrected relative to standards NBS-28 quartz and UWG-2 garnet (Valley et al., 1995). Garnets analyzed for core/rim $\delta^{18}\text{O}$ were ≥ 5 mm in diameter. Core and rim compositions were extracted using a dentist's drill, taking care to avoid inclusions, and the powders analyzed by laser fluorination. All mineral separate $\delta^{18}\text{O}$ analyses were performed in duplicate or triplicate, except where indicated (EA1), with a precision of $\leq 0.2\text{‰}$.

Uranium-lead analyses of zircon core and rim compositions were made using the SHRIMP-RG ion microprobe at Stanford University and are presented in the electronic annex (EA3). Analytical and data reduction procedures followed those given in Williams (1998). All reported ages were determined using the data-reduction program Squid (Ludwig, 2001). Common Pb corrections were made using the two-stage average crustal Pb model of Stacey and Kramers (1975).

3. RESULTS AND DISCUSSION

Our SIMS $\delta^{18}\text{O}$ results are presented on Tables 2–4, together with U concentrations, ages, and degrees of concordance. All SIMS oxygen isotope analyses are tabulated in the electronic annex (EA4). Although no overall regularity of the $\delta^{18}\text{O}$ distribution can be discerned, a closer consideration of sample-by-sample analyses reveals some general trends.

3.1. Sample IG2D-01

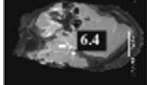
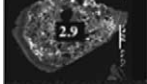
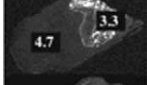
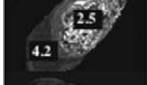
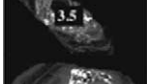
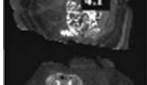
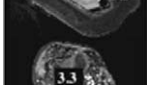
This sample was analyzed in the greatest detail and is the most useful guide to understanding the relationship between U-Pb discordance and $\delta^{18}\text{O}$ in zircon, particularly when combined with our more detailed isotopic study of the IG2D-01 outcrop. On this mount, the zircons were imaged by cathodoluminescence before U-Pb analysis. Three CL textures were recognized (Fig. 3): (A) brightly luminescent parts of a grain in which crystal faces, zoning, or twinning can be detected; (B) mottled luminescence characterized by an irregular pattern of whole grains, or grain cores in which very small dark areas are irregularly dispersed in a lighter mass; and (C) dark nonluminescent rims surrounding either textural types A or B. These groups also hold roughly constant when grouped by $\delta^{18}\text{O}$ value, and U-Pb discordance, as seen below.

3.1.1. Results

Collectively, 21 spots on 12 grains of IG2D-01 were analyzed for $\delta^{18}\text{O}$ (Table 2), three grains in duplicate or triplicate. Measurements of core-rim pairs were made on 7 grains (Table 2). Probability distribution curves for $\delta^{18}\text{O}$ in IG2D-01 zircons (Fig. 2) clearly indicate a nonunimodal distribution and an overall variation more than twice the external reproducibility for reference zircon AS57. Moreover, based on CL imaging, three texturally distinct groups are evident in sample IG2D-01 that correlate with $\delta^{18}\text{O}$ values and U-Pb ages. (1) The highest $\delta^{18}\text{O}$ values range between 5.9‰ and 6.4‰, and are characteristic of textural group A zircons. While there are only three such measurements, from three different grains, their correspondence with structural type is reciprocal—all isotopically heavy zircons are of textural group A, and all textural group A zircon $\delta^{18}\text{O}$ values are between 5.9‰ and 6.4‰, indistinguishable from the average value for zircon in TTG rocks (Tonalite, Trondhjemite, Granodiorites) of $5.6\text{‰} \pm 0.5\text{‰}$ (Peck et al., 2000). These isotopically heavy zircons also yield concordant U-Pb ages ($<20\%$ discordance) and plot on the concordia above 450 Ma, close to the upper discordia intercept (Fig. 3). (2) The lowest $\delta^{18}\text{O}$ values range from 2.5‰ to 3.6‰, with an average value of $3.3\text{‰} \pm 0.4\text{‰}$ ($n = 12$), and are characteristic of textural group B zircons. Again the $\delta^{18}\text{O}$ correspondence with texture is reciprocal. The U-Pb ages of this group are all discordant, generally exceeding 30% discordance. On a concordia diagram they plot as moderately discordant points (Fig. 3) with the exception of grain 3, which is relatively concordant (7% discordance) but exhibits a B-type texture. (3) A final group of zircons has $\delta^{18}\text{O}$ intermediate between the first two groups: 3.3‰ to 5.2‰ (one duplicate of grain #6 is 3.1‰). These are primarily of group C texture—dark nonluminescent rims—and yield U-Pb ages of 13–15 Ma, plotting close to the lower intercept on the concordia diagram (Fig. 3).

The complicated tectonic and metamorphic history expressed in the $\delta^{18}\text{O}$, U-Pb discordance, and textural domains of these zircons prompted us to take a closer look at sample IG2D-01 on an outcrop scale. In particular, we focused on oxygen isotopes of whole rock and mineral separates within and around IG2D-01. $\delta^{18}\text{O}$ values are presented in Figure 4 and summarized below. All laser and conventional fluorination $\delta^{18}\text{O}$ measurements are reported in EA1.

Table 2. Sample IG2D-01: SIMS $\delta^{18}\text{O}$ zircon core and rim analyses, together with CL images and U-Pb isotopic data. All U-Pb data represent zircon core compositions.

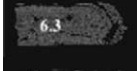
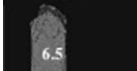
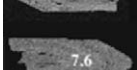
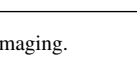
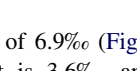
IG2D-01 Grain	$\delta^{18}\text{O}$ (‰) and CL image	U (ppm)	207corr 206Pb/238U Age $\pm 1\sigma$ (Ma)	discordance (%)
1		2460	321.5 \pm 0.9	36
2		393	449.5 \pm 2.7	2
3		4813	461.7 \pm 0.8	7
4		1383	122.8 \pm 0.6	218
5		2345	254.4 \pm 0.8	75
6		415	473.1 \pm 3.2	3
7		2184	331.2 \pm 1.1	36
8		1430	365.0 \pm 1.2	28
9		1893	26.3 \pm 0.2	285
10		2640	277.2 \pm 1.2	68
11		531	468.4 \pm 2.1	12
12		955	14.9 \pm 0.2	1750

A 100-m section of garnet amphibolite encloses IG2D-01 and is strongly depleted in ^{18}O ($\delta^{18}\text{O}_{\text{WR}} = -4.4\text{‰}$; Fig. 4). Whole rock analyses were made on a ~ 2 kg rock sample ground into a homogeneous powder. However, we cannot be certain that this sample is representative of the entire section. A concordant quartz vein hosted by the amphibolite and located a few meters from the amphibolite sample was analyzed, yielding a $\delta^{18}\text{O} = -0.4\text{‰}$ (Fig. 4, EA1), indicating that most of the amphibolite section is probably characterized by low $\delta^{18}\text{O}$. This low $\delta^{18}\text{O}$ signature must also be premetamorphic, because negative $\delta^{18}\text{O}$ values are expressed in the cores of garnets from the amphibolite (-5.0‰ , -5.4‰). Rims of the garnets are also light (-4.3‰ and -5.8‰). However, the cause for such a large variation is not entirely clear, especially considering that

one rim is lighter and the other rim is heavier than its respective core. It is possible that these garnet rims experienced different degrees of postmetamorphic re-equilibration with the amphibolite matrix. Another possibility is that metamorphic temperatures were changing during the time over which garnet growth occurred, and therefore different quartz-garnet fractionation factors are reflected in the isotopic compositions of the garnet rims. $\delta^{18}\text{O}$ for quartz separated from the amphibolite is -2.1‰ . All of these values are anomalous for Namche Barwa schists and gneisses, which exhibit a range of $\delta^{18}\text{O}_{\text{WR}}$ between 5.9‰ and 11.5‰ .

IG2D-01 itself is a deformed pegmatite dike, primarily composed of quartz (60%), plagioclase (An_{20} , 25%), almandine-rich garnet (10%), and biotite (5%). The whole rock has a

Table 3. Sample SG04744: SIMS $\delta^{18}\text{O}$ individual zircon analyses, together with BSE images and U-Pb isotopic data.

SG04744 Grain	$\delta^{18}\text{O}(\text{‰})$ and BSE image	U (ppm)	207corr 206Pb/238U Age $\pm 1\sigma$ (Ma)	discordance (%)
1		708	1411.0 \pm 14.9	41
2		717	1468.4 \pm 15.4	39
3		625	1401.8 \pm 14.8	41
4		755	1504.2 \pm 15.9	37
5		708	1668.3 \pm 17.2	32
6		515	1273.9 \pm 14.5	48
7		866	1363.9 \pm 14.4	38
8		699	1319.3 \pm 14.4	45
9		1060	1165.3 \pm 14.5	45
10		519	1997.6 \pm 20.4	22
11		972	1744.3 \pm 17.7	28
12		1699	1227.4 \pm 12.9	43
13		1378	1034.8 \pm 11.1	46
14		375	2609.9 \pm 25.8	2
16		198	2645.6 \pm 27.5	1
18		146	2472.3 \pm 26.9	7
19		276	2723.7 \pm 27.0	2

* Grain lost prior to BSE imaging.

relatively normal $\delta^{18}\text{O}_{\text{WR}}$ of 6.9‰ (Fig. 4). Quartz $\delta^{18}\text{O}$ for IG2D-01 is 7.0‰, garnet is 3.6‰, and feldspar is 4.2‰. Garnets from the pegmatite were smaller (2–3 mm) than the amphibolite garnets, and therefore core/rim comparisons of $\delta^{18}\text{O}$ were not possible.

3.1.2. Interpretation

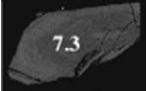
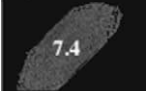
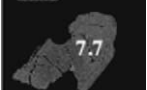
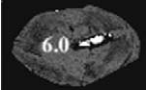
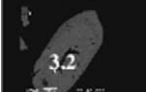
In attempting to understand these results, we begin with several precepts.

(1) Equilibrium fractionation of oxygen isotopes between minerals and water follow (Bottinga and Javoy, 1973):

$$1000 \ln \alpha \approx \Delta_{\text{Zr-water}} = \delta^{18}\text{O}_{\text{Zr}} - \delta^{18}\text{O}_{\text{H}_2\text{O}} = A + B10^6/T^2 \quad (1)$$

Krylov et al. (2002) suggested a best value of -3.71 for A and 2.75 for B, or constraining A to -3.7 (Bottinga and Javoy, 1973) B would be 2.74. Because we are not interested (nor are we able to suggest) precise thermometry, we are more concerned with the approximate values of A and B

Table 4. Sample SG04744: SIMS $\delta^{18}\text{O}$ individual zircon analyses, together with BSE images and U-Pb isotopic data.

SG04746 Grain	$\delta^{18}\text{O}$ (‰) and BSE image	U (ppm)	207corr 206Pb/238U Age $\pm 1\sigma$ (Ma)	discordance (%)
1		154	1753.0 \pm 13.0	55
2		158	2078.2 \pm 13.6	31
5		199	1322.2 \pm 8.3	104
6		112	2275.8 \pm 17.6	22
9		521	2275.8 \pm 7.7	22
11		85	2650.8 \pm 18.3	5
13		135	2829.8 \pm 15.8	0
15		798	1500.7 \pm 3.9	51

* Grain lost prior to BSE imaging.

and with the form of the equation, rather than with the precise values of its coefficients. Similarly, following Matthews et al. (1983), Valley et al. (2003) has suggested that for mineral-mineral fractionations, the A term becomes

zero, so that for zircon-quartz fractionation the equation will be

$$1000 \ln (\alpha_{\text{Zr-qz}}) \approx \Delta_{\text{Zr-qz}} = \delta^{18}\text{O}_{\text{Zr}} - \delta^{18}\text{O}_{\text{qz}} = B_{\text{Zr-qz}} 10^6 / T^2 \quad (2)$$

for which he proposes $B = 2.64$.

(2) Tomaschek et al. (2003) studied age relations, morphology, and internal structures of zircons from Syros Island in the Cyclades. They distinguished between (a) “pristine” colorless zircons with clear simple CL images, sometimes exhibiting sector zoning, which were considered to be of magmatic origin, the U-Pb age representing original crystallization, and (b) “porous” zircons, exhibiting a mottled CL texture, interpreted to represent products of dissolution-reprecipitation. This interpretation is supported by the observation of Putnis (2002) that recrystallization of this nature is accompanied by the creation of porosity, which they show (through BSE and SEM images) to be enhanced in mottled zircons.

The textural similarity between the zircons observed by Tomaschek et al. (2003) and those of IG2D-01 implies that we can also distinguish between several types of zircons:

(1) Fresh, pristine zircons, with bright CL (textural type A): These have the highest $\delta^{18}\text{O}$ and close to concordant ages of 450 Ma. They are products of pristine magmatic crystallization, representing an original crustal melt.

(2) “Mottled” zircons (textural type B): These have the lowest $\delta^{18}\text{O}$ and they are discordant. They are the result of

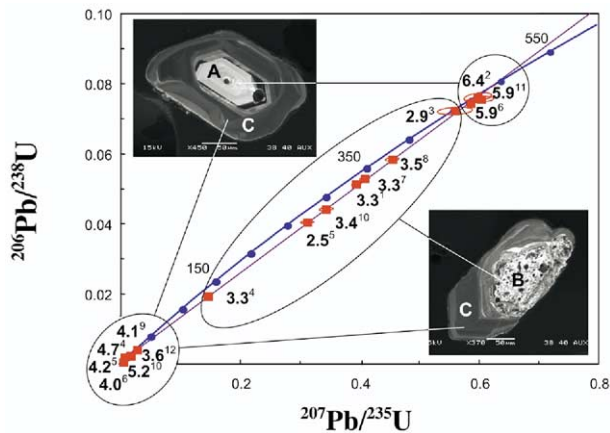


Fig. 3. U-Pb concordia diagram for sample IG2D-01, labeled with SIMS $\delta^{18}\text{O}$ analyses for each zircon spot. Grain numbers (from Table 2) are indicated in superscript typeface. Representative zircon textures for group A (smooth, brightly luminescent), group B (mottled, recrystallized), and group C (smooth, non-luminescing) are shown, as well as their rough correlation with position on the discordia.

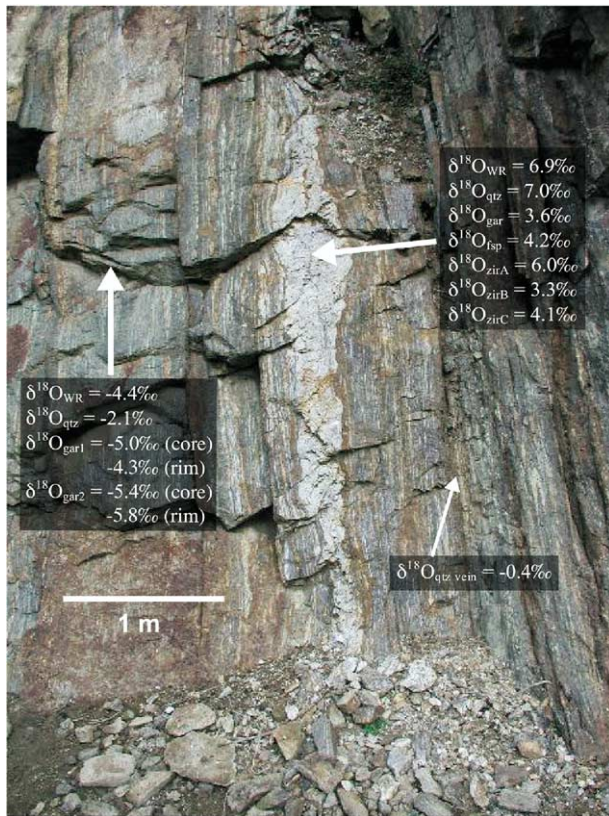


Fig. 4. Outcrop photo of IG2D-01 (deformed pegmatite dike) intruding low- $\delta^{18}\text{O}$ amphibolite, labeled with $\delta^{18}\text{O}$ results of mineral separate and whole-rock analyses for both rock types. The $\delta^{18}\text{O}$ of a concordant quartz vein is also shown. Details of the laser fluorination analyses are tabulated in EA1.

dissolution-recrystallization of igneous cores of zircons in contact with meteoric-derived fluids during the beginning of uplift at ~ 14 Ma.

(3) “Dark” zircons (textural type C): These zircons lack strong CL luminescence, have $\delta^{18}\text{O}$ that is intermediate between types A and B, and plot near the lower, very young (14 Ma or less) intercept of the discordia line. We consider them to be the product of late overgrowth on preexisting zircon cores. This scenario explains the observation that in some zircons of IG2D-01 the $\delta^{18}\text{O}$ of the rim is lighter than the core but in other grains it is heavier.

Th/U ratios are substantially lower for the rims than for unaltered cores in IG2D-01 zircons. Average Th/U for type C (rim) zircon is 0.03 ± 0.008 (1σ), as opposed to 0.54 ± 0.07 (1σ) for type A (unaltered core) zircon, suggesting that type C zircon is metamorphic in origin (EA3). Williams and Claesson (1987) first used Th/U ratios to distinguish between primary igneous zircon and metamorphic overgrowths, noting that Th/U ratios of 0.1–1.5 are characteristic of igneous zircon, whereas metamorphic overgrowths exhibit much lower values of 0.01–0.1. Metamorphic fluids are characterized by low Th/U ratios, owing to preferential leaching of U relative to Th from an orthogneiss during prograde metamorphism (Rollinson and Windley, 1980). Low Th/U ratios in the intergranular fluid, combined with the preferential partitioning of U with respect to

Th into precipitating zircon, produces metamorphic overgrowths with much lower Th/U ratios than the magmatic value (Mojzsis and Harrison, 2002). Type B (altered core) zircon from IG2D-01 has an average Th/U ratio intermediate between A and C, with very large variation among values (0.20 ± 0.26 (1σ)).

3.1.3. Tectonic history

Keeping in mind the implications that texture has for growth mechanisms, in addition to the fractionation between zircon and coexisting minerals (i.e., Valley et al., 2003), we propose the following history for IG2D-01.

(1) Early formation of a basalt protolith, which exchanged with low- $\delta^{18}\text{O}$ meteoric water. The basalt was later buried and underwent amphibolite-facies metamorphism, at which point the low- $\delta^{18}\text{O}$ signature became locked in. Dehydration during prograde metamorphism would not have substantially changed the rock’s oxygen isotopic composition, because fractionation of ^{18}O during dehydration is $<1\text{‰}$ (Valley, 1986). The age of the protolith is unknown, because neither zircon nor monazite is present in the amphibolite. Metamorphic sphenes yield a Th-Pb age of 18.3 ± 9.1 Ma. However, we know from cross-cutting relations that the amphibolite must be older than the upper intercept of the IG2D-01 discordia (450–500 Ma).

(2) Intrusion of the pegmatite (IG2D-01) at ~ 450 Ma into the low- $\delta^{18}\text{O}$ amphibolite, and crystallization of pristine igneous zircon. The source of this pegmatite is most likely a crustal melt, similar to other granitic melts present in this area (Booth et al., 2004). Clearly the pegmatite is not a local melt, because the difference between the $\delta^{18}\text{O}$ of the host rock and the pegmatite is so large (-4.4‰ vs. 6.9‰). These zircons now form the cores of larger grains; the preserved versions of these (textural group A) exhibit an average $\delta^{18}\text{O}$ of 6.1‰ , which is typical for crust-derived magmas (Valley, 2003).

(3) Infiltration of metamorphic fluids at ~ 14 Ma, likely at the beginning of uplift, which is the approximate age of metamorphism and anatexis in this area (Booth et al., 2004), causing recrystallization of select zircon cores into the polygranular texture of group B (Fig. 3). These fluids were low in $\delta^{18}\text{O}$ owing to intracommunication with the surrounding amphibolite under low fluid/rock ratio conditions. Thus the recrystallized cores of preexisting zircons acquired low $\delta^{18}\text{O}$ values (2.5‰ – 3.6‰) and partially lost Pb. At this time, other minerals in the pegmatite must have acquired low $\delta^{18}\text{O}$ as well. These values, however, were overprinted during subsequent stages of uplift/metamorphism, so the measured $\delta^{18}\text{O}$ (Fig. 4) for minerals in the pegmatite reflect the last stage of water-rock interaction. Zircons are particularly retentive of their oxygen isotopic composition owing to very slow oxygen diffusion rates, such that $\delta^{18}\text{O}$ measurements in zircon can “see through” granulite-facies metamorphism and partial melting (Peck et al., 2003). Thus the recrystallized zircon cores preserve an event not otherwise apparent through analysis of coexisting minerals. Another notable feature of the recrystallized cores is that they are all high in uranium (>1000 ppm). It is possible that metamictization of these cores made them especially susceptible to this alteration/recrystallization event, accompanied by lead loss.

There are too many degrees of freedom in such a scenario to

define accurately the $\delta^{18}\text{O}$ and temperature of such interaction. Equation 1 suggests that at $\sim 700^\circ\text{C}$ water-zircon fractionation should be close to zero and therefore water should have attained $\delta^{18}\text{O}$ of $\sim 3\text{‰}$ – 4‰ . Such a value might have been achieved by a proper water/rock ratio before zircon recrystallization, as mentioned above.

(4) Growth of zircon rims of textural type C. As uplift of the massif continued and temperature dropped, the rock continued to be infiltrated by U-rich metamorphic fluids, raising the fluid/rock ratio. Infiltration of U-rich fluids during uplift has been observed in other similar areas of the Himalayas (Chamberlain et al., 2002). The new generation of zircon (textural group C) that crystallized around preexisting grains was enriched in U, consistent with their suppressed cathodoluminescence. In some cases, new zircon growth surrounded pristine igneous zircon cores, and in other cases around recrystallized cores. $\delta^{18}\text{O}$ of the new zircon was $\sim 4\text{‰}$. We assume that as they grow during a high-temperature process, pristine granitoid zircons should have a $\delta^{18}\text{O}$ ~ 1 – 2‰ lighter than unaltered whole rock (Eqn. 2; Bibikova et al., 1982; Valley, 2003). $\delta^{18}\text{O}$ of the whole rock IG2D-01 is 6.9‰ (Fig. 4) and hence it is not unreasonable to accept the 4.1‰ average value for textural group C zircons as representative of high-T metamorphic overgrowths in equilibrium with the bulk rock. $\delta^{18}\text{O}$ values for other minerals in the pegmatite (see Fig. 4) also indicate equilibrium with group C zircon: $\Delta_{\text{qtz-zirC}} = 2.9\text{‰}$ and $\Delta_{\text{gar-zirC}} = -0.5\text{‰}$, consistent with equilibration at $\sim 700^\circ\text{C}$ (Valley et al., 2003).

The proposed scenario is in accord with the proposition of Mezger and Krogstad (1997) that zircons lose Pb only when they become metamict or during new growth of zircons. The geologic setting of the described uplift-related resetting of the U-Pb system is also similar to the dilatancy model of Goldich and Mudrey (1975) that attributes exhumation and decreased confining pressure to ages of lower discordia intercepts. We use the insights gained from IG2D-01 to help interpret the following older, and less clear-cut, samples.

3.2. Sample SG04744

3.2.1. Results

Spot analyses from 15 individual zircons of sample SG04744 yielded $\delta^{18}\text{O}$ values between 6.3‰ and 8.7‰ (Table 3). The most striking feature of the oxygen isotopic variation is that the zircons plotting on or near the concordia with less than 10% discordance (at or below the upper intercept of 2675 ± 19 Ma, grains #14–19, Table 3 and Fig. 5) have the highest $\delta^{18}\text{O}$ values (average of $8.2\text{‰} \pm 0.5\text{‰}$ (1σ)). By contrast, the average value of the discordant grains is $6.8\text{‰} \pm 0.4\text{‰}$ (1σ).

In BSE images, a textural difference is evident between the concordant and the discordant zircon grains (Table 3; Fig. 5). Whereas all discordant grains exhibit sharp euhedral oscillatory zoning, often accompanied with conspicuous microcracking of the grain, the concordant grains have more vague zoning, possibly sector zoning, that does not follow sharp crystal faces, with much less cracking. This is somewhat similar to Pidgeon's (1992) results that correlated discordance with pronounced zoning textures.

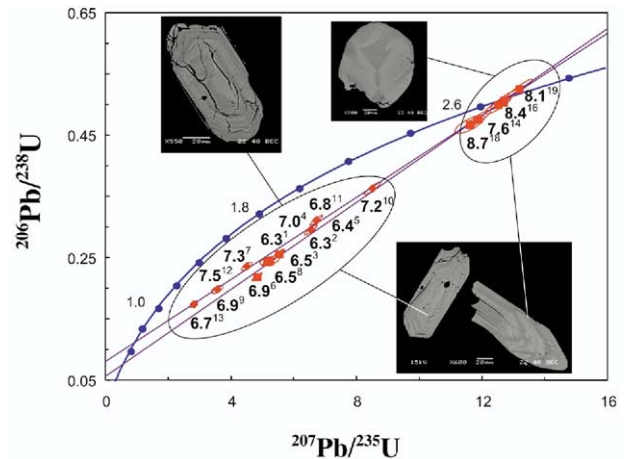


Fig. 5. U-Pb concordia diagram for sample SG04744, labeled with SIMS $\delta^{18}\text{O}$ analyses for each zircon spot. Grain numbers (from Table 3) are indicated in superscript typeface. Representative textures for discordant and concordant grains are shown.

3.2.2. Interpretation

In the case of SG04744, the difference between the sharply zoned crystals and the barely sector-zoned crystals must be one of average atomic number (Z), the major factor affecting BSE imaging. It is likely that the sharp zoning results from partial alteration or metamictization, which in turn resulted in destruction of the zircon lattice, admitting lower-Z elements and possibly water molecules. These zones are dark on a BSE image and result in greater discordance in the zoned crystals as well as depletion to various degrees in ^{18}O . The reduction in $\delta^{18}\text{O}$ is not directly dependent on the degree of discordance; instead, it is a function of the accessibility of a given zircon to the aqueous solution. The $\delta^{18}\text{O}$ values of the discordant zircons are therefore irregular in their distribution.

The lighter $\delta^{18}\text{O}$ values of the sharply zoned crystals indicate that this sharp zoning is a secondary rather than a primary feature. A likely scenario for SG04744 is that hot ($>100^\circ\text{C}$) meteoric water interacted with preexisting igneous zircons; the solution apparently intruded zircons along crystal growth planes, microcracks, and cleavage planes, thus lowering the average atomic number of the matrix and enhancing the visibility of zoning in BSE. It is not known when the $^{18}\text{O}_{\text{zircon}}$ was exchanged with this meteoric fluid and Pb was leached. Two concordia lines can be fitted to the U/Pb data (Fig. 5): one with a lower intercept of 483 ± 79 Ma and the other at 690 ± 48 Ma. Therefore, interaction(s) between meteoric water and SG04744 most likely occurred between 700 and 450 Ma.

3.3. Sample SG04746

Zircons from this sample plot on a discordia with an upper intercept of 2790 ± 31 Ma and a lower intercept of $\sim 300 \pm 200$ Ma (Fig. 6). Only eight grains were found suitable for analysis. Of those eight, the $\delta^{18}\text{O}$ values of seven grains are tightly grouped, yielding an average of $7.1\text{‰} \pm 0.5\text{‰}$ (1σ). Because of the tight grouping, no relationship can be discerned between $\delta^{18}\text{O}$ and position on the discordia. The eighth grain

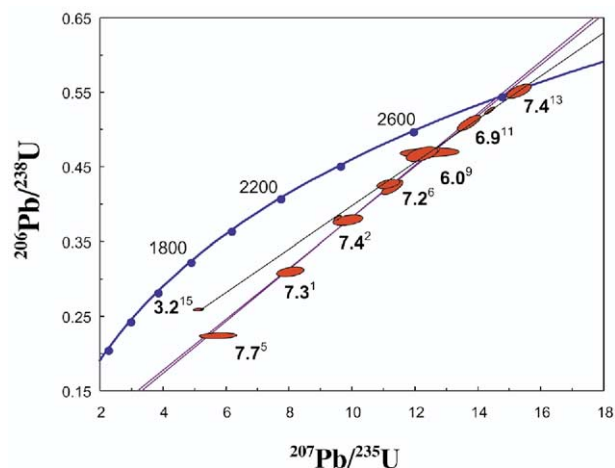


Fig. 6. U-Pb concordia diagram for sample SG04746, labeled with SIMS $\delta^{18}\text{O}$ analyses for each zircon spot. Grain numbers (from Table 4) are indicated in superscript typeface.

plots sharply off the discordia and is strongly depleted in ^{18}O ($\delta^{18}\text{O} = 3.9\text{‰}$).

The BSE images of zircons in sample SG04746 (Table 4) have mostly similar appearance, and seem to resemble all the concordant zircons in sample SG04744. The textural similarity holds true with ^{18}O composition, because there is no discernable difference in $\delta^{18}\text{O}$ between the concordant and the discordant zircon grains. The BSE image uniformity includes grain #15, definitely an outlier both with respect to its U/Pb systematics (see Fig. 6) and in its low $\delta^{18}\text{O}$. One possibility is that our $\delta^{18}\text{O}$ analysis was performed on the central dark area in the BSE image that might have been intensively altered so that the U/Pb system in the entire grain was disturbed.

4. SUMMARY

We have attempted to link three characteristic features of zircons that are not self-evidently interrelated: (1) U/Pb systematics and the associated age discordance, (2) $\delta^{18}\text{O}$ signature and its evidence for water-rock interaction, and (c) zircon zoning textures as revealed by CL and BSE imaging. A key observation is that U-Pb-disturbed zircons are often also variably depleted in ^{18}O . Together with this is the visual documentation of different stages of water-rock interaction, seemingly imprinted on the texture of a zircon. Thus the IG2D-01 zircons from Tibet record in their $\delta^{18}\text{O}$ values original magmatic crystallization, recrystallization in the presence of meteoric waters, and a high-temperature metamorphic overgrowth event. An additional lesson we might draw from our ion probe analyses is that, often, “zircons are forever,” in the sense that, unlike in other phases, later events will not erase the memory of earlier ones. However, it is clear from our results that sometimes such erasing can occur. The record of several events in a single zircon population, including recrystallization events, indicates that perhaps “zircons are not forever.” This has been previously suggested by the oxygen isotopic studies of Bindeman and Valley (2000, 2001, 2003) on zoned zircons from Yellowstone.

The Archean rocks from the Victoria Greenstone Belt

(SG04744 and SG04746) also record a later low-temperature “hydrothermal” event, although strong depletions in ^{18}O are rare compared to the Tibetan sample. In sample SG04744, this hydrothermal overprint is expressed as enhanced sharp zonations in BSE images. In both the Tibetan and Archean cases, textural development is a secondary phenomenon. This has clear implications for routine geochronologic applications, where preference is often given to the zoned, presumably most pristine, zircon crystals. Our results suggest that this practice should be viewed with caution, in the sense that fine concentric banding of the type exhibited by sample SG04744 (grains #1–13, Table 3) may point to a secondary origin that is associated with age discordance and ^{18}O depletion.

Acknowledgments—This research was greatly aided by the advice of L. T. Silver. We also thank Marty Grove and Kevin McKeegan for help with the SIMS at UCLA, Frank Mazdab for assistance on the SHRIMP-RG, and Richard Tosdal for supplying sample mounts SG04744 and SG04746. John Valley and an anonymous reviewer are thanked for their thoughtful reviews and suggestions, along with James Farquhar for editorial handling. In particular, John Valley’s detailed comments and communication were of immense help, and significantly improved the manuscript. This work was supported in part by NSF grant EAR-0003530–002 awarded to C. P. Chamberlain. The ion microprobe facility at UCLA is partly supported by a grant from the Instrumentation and Facilities Program, Division of Earth Sciences, National Science Foundation.

Associate editor: James Farquhar

REFERENCES

- Bibikova Y. V., Ustinov V. I., Gracheva T. V., Kiselevskiy M. A., and Shukolyukov Y. A. (1982) Variations of isotopic composition of oxygen in accessory zircons. *Doklady Akademii Nauk SSSR* **264**, 698–700.
- Bindeman I. N. and Valley J. W. (2000) Formation of low- $\delta^{18}\text{O}$ rhyolites after caldera collapse at Yellowstone, Wyoming, USA. *Geology* **28**, 719–722.
- Bindeman I. N. and Valley J. W. (2001) Low- $\delta^{18}\text{O}$ rhyolites from Yellowstone; magmatic evolution based on analyses of zircons and individual phenocrysts. *J. Petrol.* **42**, 1491–1517.
- Bindeman I. N. and Valley J. W. (2003) Rapid generation of both high- and low- $\delta^{18}\text{O}$, large-volume silicic magmas at the Timber Mountain/Oasis Valley caldera complex, Nevada. *Geol. Soc. Am. Bull.* **115**, 581–595.
- Booth A. L., Zeitler P. K., Kidd W. S. F., Wooden J., Lui Y., Idleman B., Hren M., and Chamberlain C. P. (2004) U-Pb zircon constraints on the tectonic evolution of southeastern Tibet, Namche Barwa area. *Am. J. Sci.* **304**, 889–929.
- Borg G. and Shackleton R. M. (1997) The Tanzania and NE-Zaire cratons. In: *Greenstone Belts* (eds. M. J. De Wit and L. D. Ashwal), Oxford Monographs on Geology and Geophysics, Vol. 35, pp. 608–619.
- Bottinga Y. and Javoy M. (1973) Comments on oxygen isotope geothermometry. *Earth Planet. Sci. Lett.* **20**, 250–265.
- Chamberlain C. P., Koons P. O., Meltzer A. S., Park S. K., Craw D., Zeitler P. K., and Poage M. A. (2002) Overview of hydrothermal activity associated with active orogenesis and metamorphism; Nanga Parbat, Pakistan Himalaya. *Am. J. Sci.* **302**, 726–748.
- Connelly J. N. (2000) Degree of preservation of igneous zonation in zircon as a signpost for concordancy in U/Pb geochronology. *Chem. Geol.* **172**, 25–39.
- Davis D. W., Williams I. S., and Krogh T. S. (2003) Historical development of zircon geochronology. In *Zircon*: (eds. J. M. Hanchar and P. W. O. Hoskin), Reviews of Mineralogy & Geochemistry, Vol. 53, pp.145–181.

- Eiler J. M., Graham C. M., and Valley J. W. (1997) SIMS analysis of oxygen isotopes: Matrix effects in complex minerals and glasses. *Chem. Geol.* **138**, 221–244.
- Fayek M., Harrison T. M., Ewing R. C., Grove M., and Coath C. D. (2002) O and Pb isotopic analyses of uranium minerals by ion microprobe and U-Pb ages from the Cigar Lake Deposit. *Chem. Geol.* **185**, 205–225.
- Goldich S. S. and Mudrey M. G. Jr. (1975) Dilatancy model for discordant U-Pb zircon ages. In: *Recent contributions to geochemistry and analytical chemistry* (ed.: A. I. Tugarinov).
- Krylov D. P., Zagnitko V. N., Hoernes S., Lugovaja I. P., and Hoffbauer R. (2002) Oxygen isotope fractionation between zircon and water: Experimental determination and comparison with quartz-zircon calibrations. *Eur. J. Mineral.* **14**, 849–853.
- Ludwig K. R. (2001) User's Manual for Isoplot/Ex, Version 2.49, A Geochronological Toolkit for Microsoft Excel. Berkeley Geochronology Center Special Pub. No. 1a, 55, p.
- Mathews A., Goldsmith J. R., and Clayton R. N. (1983) Oxygen isotope fractionations involving pyroxenes: The calibration of mineral-pair geothermometers. *Geochim. Cosmochim. Acta* **47**, 631–644.
- Mezger K. and Krogstad E. J. (1997) Interpretation of discordant U-Pb zircon ages: An evaluation. *J. Metamorphic Geol.* **15**, 127–140.
- Mojsis S. J. and Harrison T. M. (2002) Establishment of a 3.83 Ga magmatic age for the Akilia tonalite (southern West Greenland). *Earth Planet. Sci. Lett.* **202**, 563–576.
- Peck W. H., King E. M., and Valley J. W. (2000) Oxygen isotope perspective on Precambrian crustal growth and maturation. *Geology* **28**, 363–366.
- Peck W. H., Valley J. W., Wilde S. A., and Graham C. M. (2001) Oxygen isotope ratios and rare earth elements in 3.3 to 4.4 Ga zircons: Ion microprobe evidence for high $\delta^{18}\text{O}$ continental crust and oceans in the early Archean. *Geochim. Cosmochim. Acta* **65**, 4215–4229.
- Peck W. H., Valley J. W., and Graham C. M. (2003) Slow oxygen diffusion rates in igneous zircons from metamorphic rocks. *Am. Mineral.* **88**, 1003–1014.
- Pidgeon R. T. (1992) Recrystallisation of oscillatory zoned zircon: some geochronological and petrological implications. *Contrib. Mineral. Petrol.* **110**, 463–472.
- Pidgeon R. T., Nemchin A. A., and Hitchen G. J. (1998) Internal structures of zircons from Archaean granites from the Darling Range batholith: Implications for zircon stability and the interpretation of zircon U-Pb ages. *Contrib. Mineral. Petrol.* **132**, 288–299.
- Putnis A. (2002) Mineral replacement reactions: from macroscopic observations to microscopic mechanisms. *Mineral. Mag.* **66**, 689–708.
- Riciputi L. R., Paterson B. A., and Ripperdan R. L. (1998) Measurement of light stable isotope ratios by SIMS: Matrix effects for oxygen, carbon and sulfur isotopes in minerals. *Int. J. Mass Spectrometry* **178**, 81–112.
- Rollinson H. R. and Windley B. F. (1980) Selective elemental depletion during metamorphism of Archean granulites. *Contrib. Mineral. Petrol.* **72**, 257–263.
- Sharp Z. D. (1990) A laser-based microanalytical method for the in situ determination of oxygen isotope ratios of silicates and oxides. *Geochim. Cosmochim. Acta* **54**, 1353–1357.
- Silver L. T. (1963) The relation between radioactivity and discordance in zircon. *Nucl. Phys.* **1075**, 34–39.
- Silver L. T. and Deutsch S. (1963) Uranium-lead isotopic variations in zircon; a case study. *J. Geol.* **71**, 721–758.
- Stacey J. S. and Kramers J. D. (1975) Approximation of terrestrial lead isotopic evolution by a two-stage model. *Earth Planet. Sci. Lett.* **26**, 207–221.
- Taylor H. P. Jr. (1977) Water/rock interactions and the origin of H_2O in granitic batholiths. *J. Geol. Soc. Lond.* **133**, 509–558.
- Taylor H. P. Jr. and Sheppard S. M. F. (1986) Igneous rocks: I. Processes of isotopic fractionation and isotope systematics. In *Stable Isotopes in High Temperature Geological Processes* (eds. J. W. Valley, H. P. Taylor, Jr., and J. R. O'Neil), Reviews of Mineralogy, Vol. 16, pp. 227–271.
- Tomaschek F., Kennedy A. K., Villa I. M., Lagos M., and Ballhaus C. (2003) Zircons from Syros, Cyclades, Greece: Recrystallization and mobilization of zircon during high-pressure metamorphism. *J. Petrol.* **44**, 1977–2002.
- Valley J. W. (1986) Stable isotope geochemistry of metamorphic rocks. In *Stable Isotopes in High Temperature Geological Processes* (eds. J. W. Valley, H. P. Taylor, Jr., and J. R. O'Neil), Reviews of Mineralogy, Vol. 16, pp. 445–489.
- Valley J. W. (2003) Oxygen isotopes in zircon. In *Zircon* (eds. J. M. Hanchar and P. W. O. Hoskin), Reviews in Mineralogy & Geochemistry, Vol. 53, pp. 343–385.
- Valley J. W., Chiarenzelli J. R., and McLelland J. M. (1994) Oxygen isotope geochemistry of zircon. *Earth Planet. Sci. Lett.* **126**, 187–206.
- Valley J. W., Kitchen N. E., Kohn M. J., Niendorf C. R., and Spicuzza M. J. (1995) UWG-2, A garnet standard for oxygen isotope ratio: Strategies for high-precision and accuracy with laser heating. *Geochim. Cosmochim. Acta* **59**, 5223–5231.
- Valley J. W., Kinny P. D., Schulze D. J., and Spicuzza M. J. (1998) Zircon megacrysts from kimberlite: Oxygen isotope variability among mantle melts. *Contrib. Mineral. Petrol.* **133**, 1–11.
- Valley J. W., Bindeman I. N., and Peck W. H. (2003) Empirical calibration of oxygen isotope fractionation in zircon. *Geochim. Cosmochim. Acta* **67**, 3257–3266.
- Wetherill G. W. (1956) Discordant uranium-lead ages. *Trans. Am. Geophys. Union* **37**, 320–326.
- Williams I. S. (1998) U-Th-Pb geochronology by ion microprobe. In *Applications of Microanalytical Techniques to Understanding Mineralizing Processes* (eds. M. A. McKibben, W. C. Shanks, III, and W. I. Ridley), Society of Economic Geological Reviews, Vol. 7, pp. 1–35.
- Williams I. S. and Claesson S. (1987) Isotopic evidence for the Precambrian provenance and Caledonian metamorphism of high grade paragneisses from the Seve Nappes, Scandinavian Caledonides. *Contrib. Mineral. Petrol.* **97**, 205–217.

ELECTRONIC ANNEX

Supplementary data associated with this article can be found, in the online version, at doi:10.1016/j.gca.2005.05.013.